Journal of the European Ceramic Society 16 (1996) 503–513

0955-2219(95)00163-8
0955-2219/96/$15.00

Fatigue Crack Growth Rate and Fracture Toughness of 25 wt% Silicon Carbide Whisker Reinforced Alumina Composite with Residual Porosity

A. K. Ray,[a] E. R. Fuller[b] & S. Banerjee[c]

[a]National Metallurgical Laboratory, Jamshedpur–831007, Bihar, India
[b]National Institute of Standards and Technology, Gaithersburg, MD 20899, USA
[c]Research and Development Centre for Iron and Steel, SAIL, Ranchi–834002, Bihar, India

(Received 8 December 1994; revised version received 20 July 1995; accepted 28 August 1995)

Abstract

The main purpose of this study was to determine the fracture toughness and the fatigue crack growth rate behaviour of 25 wt% silicon carbide whisker reinforced alumina ceramic composite. The fracture toughness values determined using the indentation technique depended significantly on the crack length produced at the corners of the indentation which, in turn, depended on the load used for the indentation and anisotropy in orientation of whiskers in the matrix. However, the fracture toughness values determined using the precracked four-point bend specimens were in general higher than that obtained by the indentation technique and the value was 5·96 ± 0·15 MPa $m^{1/2}$. The fatigue crack growth behaviour in this material was similar to that in the case of metals. However, the exponent for the fatigue crack growth rate was 15·5, significantly higher than that usually observed in metals. The likely micromechanism of crack growth under monotonic and cyclic loading in this composite has been identified from fractography of fatigue failed samples.

1 Introduction

Silicon carbide whiskers have been incorporated in such ceramic materials as alumina to improve the general mechanical properties[1–9] and the resistance to catastrophic failure in particular. These ceramic composite materials have potential application in the production of structural components used at elevated temperatures,[10–12] i.e. in high efficiency heat engines and heat recovery systems, and for making cutting tools to machine special materials. When used in such applications, these ceramic components often encounter monotonic and cyclic loading which produces crack extension. Accordingly, in the present investigation, the fatigue crack growth behaviour (FCGR) and the fracture toughness (K_{IC}) of a high density, 25 wt% silicon carbide whisker reinforced alumina composite have been studied.

In general, the determination of FCGR and K_{IC} of such ceramic materials is difficult since the specimens are small, Young's modulus of such materials is rather high and the material is brittle. Consequently, the load, displacement and crack length — which are all required to be measured for the determination of K_{IC} and FCGR — are very small and their precise measurement poses some problems. In addition, the permissible dimensional tolerance of the specimens and those of the grips and fixtures used to test the specimens, have to be very close. Particularly difficult is the precracking of ceramic specimens since these materials have very low toughness. Moreover, the crack initiation in such materials often requires a load which is higher than that required for crack extension. Therefore specimens fail before crack growth is achieved in a controlled manner, because the precision and dimensional tolerance of the fixture used to precrack the specimens are not adequate to avoid spurious loading, that is loading in modes other than in mode I.

2 Material and Specimen Orientation

The ceramic composite material was prepared by mixing α-alumina powder of particle size < 1 μm with 25 wt% β-silicon carbide whiskers. The average whisker diameter was 0·45–0·65 μm and the length ranged from 10 to 80 μm.[8] This mixture was hot-pressed at 1700 to 1850°C under a pressure of 25 MPa for 30 min to produce a preformed billet.

The grain size of the matrix varied between 1 and 4 μm. Details of fabrication, processing and microstructural characterization are reported elsewhere.[8]

The composite material had a porosity of 4·89%, Young's modulus of 340 GPa, fracture strength of 559 MPa and a hardness of 20 GPa, as determined by National Institute of Standards and Technology (NIST), USA, and has been reported in Ref. 8.

Four-point flexure specimens, of dimensions 3 mm × 4 mm × 50 mm, were sliced from the preformed billet and were supplied to us (National Metallurgical Laboratory, NML, India) by NIST. A sketch of the billet showing the longitudinal (L), long transverse (LT) and the short transverse (ST) planes is presented in Fig. 1(a). Opposite sides of the four-point flexure specimens were diamond-ground flat and parallel with a 30 μm diamond wheel, and the prospective tensile surface was polished with 9 μm diamond paste.[8] The specimens were soaked and rinsed in ethyl alcohol to remove the wax needed to mount them for polishing, and then dried in a hot air flow.

The location and orientation of the flexure specimens in the billet is shown in Fig. 1(a). The 3 mm × 50 mm faces of the specimen were parallel to the ST plane. The crack plane introduced later in the specimen was parallel to the LT plane and the crack propagation direction was parallel to the 4 mm dimension of the specimen. Thus the direction of crack propagation was perpendicular to the hot-pressing direction. Accordingly, the crack front was parallel to the hot-pressing direction [see Fig. 1(a)]. On the other hand, in the *R*-curve studies[8] undertaken earlier by one of the authors, while the plane of crack propagation was parallel to the LT plane like in the present investigation, the direction of crack propagation was parallel to the 3 mm dimension.

A montage of the microstructures of the 25 wt% silicon carbide whisker reinforced alumina ceramic composite, as shown in Fig. 1(b), revealed a three-dimensional 3D distribution pattern of the whiskers in the L, the LT and the ST planes of the billet. As can be seen from Fig. 1(b), the distribution of the whiskers in the L plane was non-uniform and heterogeneous. The cross-section of these whiskers measured ~0·45 μm in diameter. During hot-pressing, the whiskers which were not normal to the longitudinal plane became further inclined and therefore some of the whiskers appeared to be randomly oriented in the L plane [Fig. 1(b)]. However, a majority of the whiskers tended to be oriented normal to the hot-pressing direction. Since the material flow along this plane was high, whiskers were aligned normal to this plane. On the other hand, in the ST plane, a few

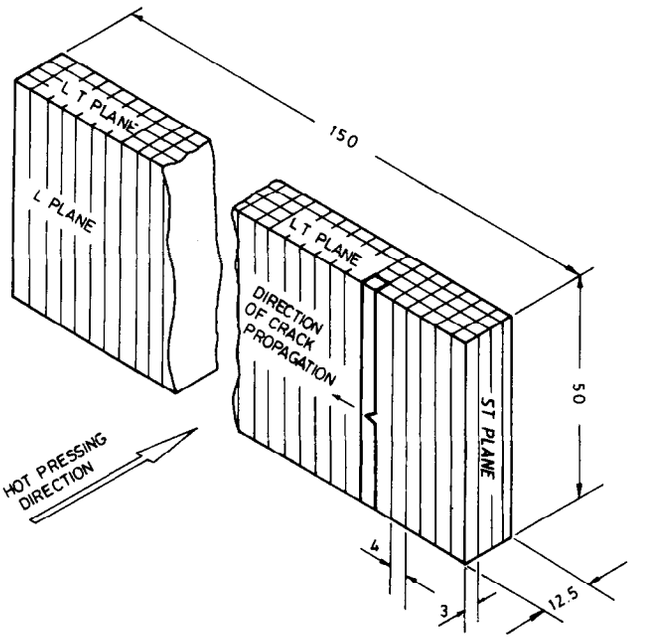

Fig. 1. (a) Billet prepared from the 25 wt% silicon carbide whisker reinforced alumina composite; (b) montage of the microstructures showing the distribution of the SiC whiskers along the three planes.

of the whiskers seemed to be embedded with random orientation; and the others were observed to be embedded normal to this plane. Probably, the friction of the walls, which in the ST planes were very close to each other, prevented easy material flow and the alignment of all the whiskers normal to the ST plane.

According to Becher and Wei,[13] whisker orientation during processing of hot-pressed SiC-whisker reinforced alumina leads to anisotropy in both fracture toughness and fracture strength of

these composites. In other words, their fracture strengths are limited by the non-uniformity of distribution of the whiskers, i.e. by the ability to disperse the SiC whiskers. They also found that dispersion of the whiskers was improved by using finer alumina powder, resulting in an increase in the fracture strength of the composite. Nevertheless, they have clearly observed[13,14] that, similar to our composite under investigation [Fig. 1(b)], the whiskers were preferentially aligned perpendicular to the hot-pressing axis. This type of distribution of whiskers suggests that a great deal of rearrangement of whiskers and powders occurred in the initial stage of densification of the composites and/or the matrix material underwent considerable deformation or creep during hot-pressing.

3 Experimental Procedure

3.1 Precracking of the specimens

The standard bridge technique is normally used for precracking four-point bend specimens. However, it did not produce satisfactory precracking and all the specimens loaded for precracking in this fixture (24 out of the 30 specimens supplied) were lost due to premature crack extension. This is probably related to fixture stiffness more than anything else. An examination of the changing crack path trajectory on the fractured surfaces of these lost specimens showed that, instead of pure mode I loading, the specimens experienced a combined mode loading with mode III loading playing a significant role in the crack extension. The bridge technique was, therefore, modified to avoid mode III loading during precracking. Accordingly, new articulated precracking bridge fixtures were designed and fabricated. These fixtures gave excellent results—achieving 100% success in precracking. The articulated bridge fixtures have been described elsewhere.[15]

A Vicker's indentation was produced at 0·8 kN load at the mid-point of the upper face (3 × 50 mm surface) of the four-point bend specimen, which acted as the crack starter. Before indention, all the specimens were coated with aluminium in a vacuum evaporator by physical vapour deposition technique to ~0·03 μm thickness, to facilitate location of the crack tip in the scanning electron microscope. Precracking was accomplished using the articulated bridge fixture at a force of 4 to 5 kN, load ratio (R) of 0·1 and frequency (f) of 20 Hz. The crack growth was measured at first on the top surface, and later on the two side surfaces, of the four-point bend specimen using the micron marker in a Jeol JSM 840A scanning electron microscope (SEM).

3.2 Crack length measurement

The crack starter indentation at the mid-point of the upper face of the specimen had cracks at all four of its corners (Fig. 2). During precracking, the crack length of the two corner cracks growing across the thickness of the specimen, which is of prime importance for the present investigation, was measured using the micron marker in the SEM at a magnification of 40×. The tip of the crack was located through observation at higher magnification, which often showed evidence of crack branching. The branch extending the furthest was considered to be the crack tip and the crack length was measured accordingly.

At first, the crack length of these two cracks growing on the tensile (3 mm × 50 mm) surface of the specimen from the two opposite corners of the indentation as crack starter, was monitored during precracking. Later, after these two cracks had spanned right across the specimen thickness, the crack lengths were measured on both the side surfaces (4 mm × 50 mm planes) from the respective upper edges. The average of the crack length measured on the side surfaces gave the crack length a.

The crack length a was measured in this manner during the precracking and also during the FCGR determination which preceded the K_{IC} testing. After the crack had advanced with regular increments of number of cycles, the specimen was unloaded from the MTS-880 servohydraulic test machine, and the current crack length was measured using the SEM. Since the determination of FCGR required precise measurement of Δa, the crack length during FCGR studies was measured with special care taken in locating the crack tip.

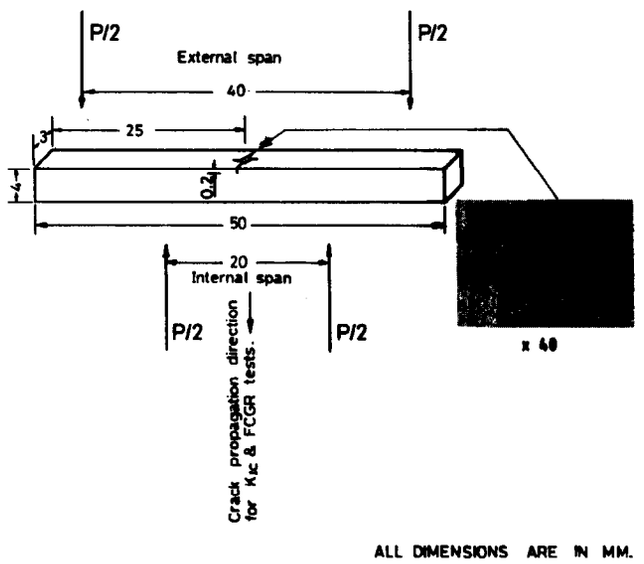

Fig. 2. Indented and precracked specimen for four-point bend loading. Cracks are located at the four corners of the indentation.

3.3 Determination of fatigue crack growth rate (FCGR)

FCGR was determined after the crack had grown significantly on the side surfaces during precracking and achieved length a equivalent to $a/W \approx 0{\cdot}05$ to $0{\cdot}1$. The four-point bend specimen is not recommended in ASTM Standard E647 and, therefore, the K_I values of the specimen were calculated using the standard formula reported elsewhere[16,17] (referred to as the ASTM STP 410 method). Except for this aspect and the use of an indentation as a crack starter, the procedure used here to determine FCGR conformed to the recommendations given in ASTM Standard E647.

The tests were conducted in an MTS-880 servohydraulic test machine using a 1 kN load cell under four-point bend loading, in laboratory atmosphere and at ambient temperature. The loading rate was $0{\cdot}25$ N s^{-1}. The frequency was 1 Hz and $R = 0{\cdot}1$. Typically, the specimens were cycled within the load range between 11 and 111 N, when $a/W \approx 0{\cdot}1$. The crack lengths were measured at regular increments of number of cycles giving ~ $0{\cdot}05$ to $0{\cdot}1$ mm of crack growth. While measuring the crack length, the specimen was first unloaded from the servohydraulic machine and the current crack length was measured with the help of the micron marker in the SEM. Thus the fatigue cracking was interrupted after a predetermined number of load cycles. This was continued until the crack length increased to a value giving $a/W \approx 0{\cdot}45$ to $0{\cdot}5$.

The test data of crack length were plotted in terms of crack length a vs. number of cycles N. The values of da/dN were generated from the a vs. N plot at any given a and plotted against ΔK (stress intensity range). With load and a known, K_I values were calculated from[16,17]

$$K_I = Y\,3P\,(L_1 - L_2)\sqrt{a / 2bW^2} \qquad (1)$$

where

$$Y = 1{\cdot}99 - 2{\cdot}47\,(a/W) + 12{\cdot}97\,(a/W)^2 - 23{\cdot}17\,(a/W)^3 + 24{\cdot}80\,(a/W)^4$$

P = load; L_1 = external span; L_2 = internal span; b = thickness of specimen; W = depth or width of specimen; a = crack length. The values of K_{max} and K_{min} were calculated using eqn (1). The ΔK value is given by $K_{max} - K_{min}$.

3.4 Fracture toughness (K_{IC}) testing

After the FCGR determination was complete and the crack had grown to a level of $a/W \approx 0{\cdot}45$ to $0{\cdot}5$, K_{IC} was determined by subjecting the precracked four-point bend specimens to monotonic loading. The test record of load vs. mid-point displacement of the specimen was obtained during monotonic loading; the ramp rate was $0{\cdot}25$ N s^{-1}. The load value corresponding to the onset of fast fracture was used in eqn (1) to obtain the K_{IC} value. Since four-point bend specimens were used, K_{IC} testing followed here conformed in all respects to the method given elsewhere.[16,17]

In addition to this procedure, the indentation fracture toughness K_C of this material was determined from the indentation technique at various loads ($0{\cdot}63$, $0{\cdot}8$, $1{\cdot}0$ and $1{\cdot}2$ kN) using the following equation proposed by Anstis *et al.*[18]

$$K_C = 0{\cdot}016\sqrt{\frac{E}{H}}\cdot\frac{P}{a^{3/2}} \qquad (2)$$

where E is the Young's modulus, H is the hardness, P is the load and a the crack length. Many emperical expressions to evaluate indentation fracture toughness have been reported in the literature.[19] However, in the case of toughened ceramics where radial cracks are emanating at the four corners of the Vickers indentation,[19] the above model [eqn (2)] has been used by Anstis *et al.*[18] to determine K_C.

3.5 SEM studies

The fracture surfaces of the test specimens were coated with a thin film of gold (thickness $0{\cdot}02$ μm) and then examined using the scanning electron microscope to identify the characteristic fractographic features of the fatigue and fast fracture regions in this material. The identification of these features gives a clue as to the likely mechanisms of fracture for this material.

At first, the SEM examination of the fatigue fracture and fast fracture zones was carried out at a low magnification of 30×. Thereafter, each of these zones was scanned at 4500× and 7500×. The fatigue crack growth at the low ΔK region and the fast fracture region (due to monotonic loading) were carefully examined in order to identify and distinguish between the characteristic fractographic features.

4 Results

4.1 Fracture toughness data

Fracture toughness values determined in this project, using both the indentation technique as well as the ASTM STP 410 method with precracked specimens, are reported in Table 1. Indentation fracture toughness test data determined with a Vickers indentation at various loads of $0{\cdot}63$, $0{\cdot}80$, $1{\cdot}0$ and $1{\cdot}2$ kN yielded K_C values of $5{\cdot}37$, $5{\cdot}45$, $5{\cdot}5$ and $5{\cdot}6$ MPa m$^{1/2}$, respectively. Figure 3 shows the variation of indentation fracture toughness values with the square root of the corresponding crack lengths. It was observed (see Fig. 3) that the

Table 1. Fracture toughness determined by indentation and by using precracked specimen for 25 wt% SiC reinforced Al_2O_3 composite

Fracture toughness (MPa $m^{1/2}$)		
Precracked specimen (ASTM STP 410 method)	*Indentation technique*	*Indentation–strength method* [8]
6·1	5·37	5·35 ± 0·17
5·8	5·45	
6·0	5·5	
	5·6	
Average: 5·96 ± 0·15	5·48 ± 0·08	

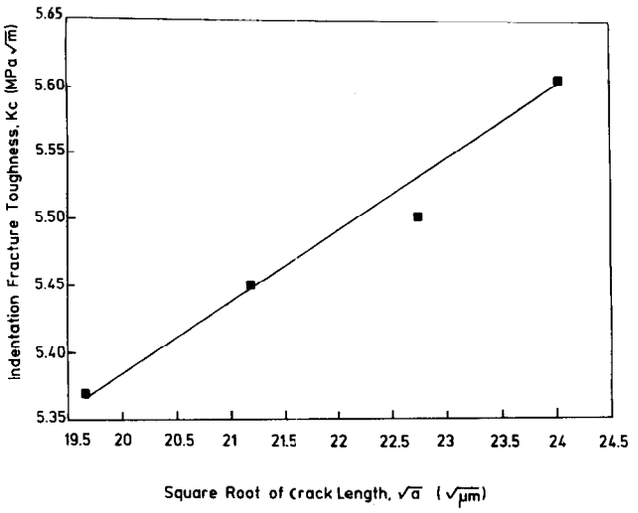

Fig. 3. Dependence of indentation fracture toughness K_C on the square root of crack length $a^{1/2}$.

indentation fracture toughness of this composite when determined using the indentation technique increased as a function of the square root of the crack length.

4.2 FCGR studies

Fatigue crack propagation behaviour of this ceramic material is reported in Fig. 4. The FCGR data of this material were fitted to the usual Paris equation $da/dN = A\ (\Delta K)^n$,[20–22] and the fatigue crack growth rate da/dN (in m/cycle) increased linearly with ΔK (in MPa $m^{1/2}$) in a log–log plot. The plot yields a value of $n = 15{\cdot}5$ and $A = 3{\cdot}4 \times 10^{-15}$ [m/cycle (MPa $m^{1/2})^{-n}$].

4.3 SEM studies

SEM fractographs of the fracture surface at the low ΔK cyclic and at monotonic loading (fast fracture region) are presented in Figs 5 to 11. It is evident that, at low ΔK (0·8 to 1·8 MPa $m^{1/2}$), a majority of the whiskers fail by producing a flat fracture surface which has a vertical level, same as the general fracture surface of the composite (see Fig. 5). On the other hand, in the fast fracture region, the whiskers fail predominantly by pull-

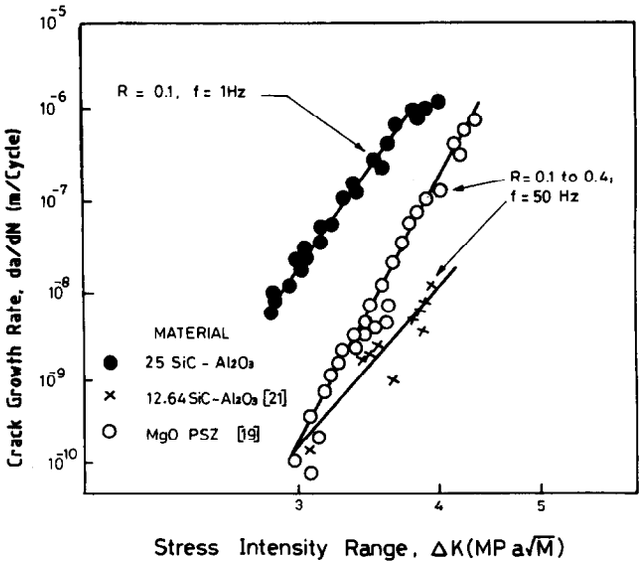

Fig. 4. Fatigue crack propagation rate data.

Fig. 5. At low ΔK (0·8 to 1·8 MPa $m^{1/2}$) region, a majority of the whiskers failed with a square fracture without evidence of large–scale pull-out.

Fig. 6. In the fast fracture region (K_{IC} = 5·9 MPa $m^{1/2}$), due to monotonic loading, whiskers failed predominantly by pull-out mechanism.

out wherein the whiskers stick out of the general fracture surface of the composite (see Fig. 6).

The matrix material failed predominantly by transgranular fracture (see Fig. 7) at low ΔK fatigue (0·8 to 1·8 MPa $m^{1/2}$). During monotonic

Fig. 7. At low ΔK (0·8 to 1·8 MPa $m^{1/2}$) region, the alumina matrix failed predominantly through transgranular fracture.

Fig. 10. Crack deflection in the low ΔK (0·8 to 1·8 MPa $m^{1/2}$) region.

Fig. 8. In the fast fracture region (K_{IC} = 5·9 MPa $m^{1/2}$), due to monotonic loading, the alumina grains failed in a mixed mode, i.e. intergranular (~55%) and transgranular (~45%).

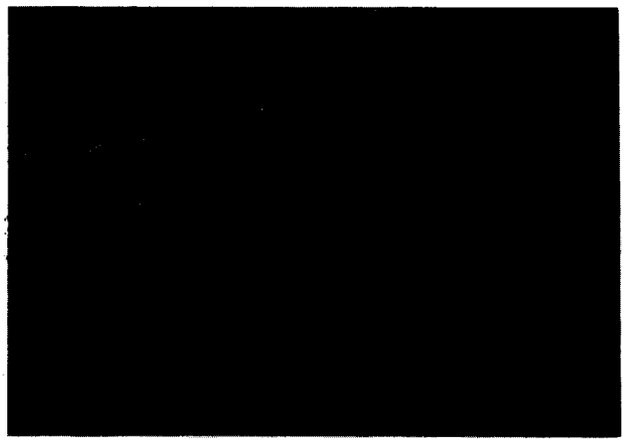

Fig. 11. River pattern marking with steps in the low ΔK (0·8 to 1·8 MPa $m^{1/2}$) region (YZ — modulation SEM image).

Fig. 9. Crack branching in the low ΔK (0·8 to 1·8 MPa $m^{1/2}$) region.

loading, the alumina grains failed in a mixed mode with about 55% by intergranular mode and the balance by transgranular mode, as shown in Fig. 8.

It is noteworthy that in the low ΔK region the crack frequently branches and deflects while it propagates (Figs 9 and 10). Correspondingly, river pattern markings with steps are also present in the cleavage facets (Fig. 11). However, in the fast fracture regions, branching and deflection of the crack are virtually absent.

The distinction between the fractographic features in the low ΔK fatigue region and the fast fracture region is very evident. This is discussed further below.

5 Discussion

5.1 Indentation fracture toughness data

In the indentation fracture toughness test, the direct crack measurement technique had been adopted[18] for obtaining a rapid assessment of the indentation fracture toughness, K_C. It can be seen from Fig. 3 that the K_C values obtained by this technique increase with increase in the square root of the corresponding crack lengths. In this context, the presence of residual stresses plays an important role. A residual compressive surface stress would decrease the apparent surface crack length, while a residual tensile surface stress would do the reverse. There are various ways in which surface stresses could be introduced into a material; of

particular relevance to the production of samples for indentation testing is the process of surface grinding brittle materials, e.g. using SiC or diamond abrasive wheels on glass, ceramics and cermets.[23] It is well documented that this surface-finishing method induces residual stresses in materials such as alumina,[23] pyroceram C9606 glass-ceramic[24] and zirconia-toughened alumina.[25]

Several investigators have shown that if the slope of the K_C (indentation fracture toughness) vs. $a^{1/2}$ (square root of crack length) plot is positive, it indicates that the nature of residual surface stress present is compressive; if the slope is negative, then tensile residual surface stresses are present.[26,27] Marshall and Lawn[26] showed that such plots for tempered soda-lime glass plate produced a positive slope indicating that the nature of residual stress is compressive. In line with the Marshall and Lawn model,[26] Ikuma and Virkar[27] thus concluded that a positive linear dependence of K_C on $a^{1/2}$ for transformation-toughenable ceramics indicates the presence of residual surface compressive stresses induced by the tetragonal-to-monoclinic transformation of ZrO_2 or HfO_2 particles in the near-surface layers upon surface grinding. Based on the same theory, since the ceramic composite under investigation here shows a positive linear dependence of K_C on $a^{1/2}$, it simply indicates that the residual surface stresses present in the composite are compressive in nature.

Ponton and Rawlings[19] concluded that in indentation fracture toughness tests although the crack length a increases with increasing indenter load P as expected, plots of K_C vs. $a^{1/2}$ do not necessarily produce a zero slope for the stress-free state, a negative slope for the residual tensile stress state and a positive slope for the residual compressive stress state, as predicted by the Marshall and Lawn model.[26] According to them,[19] the sign of the slope depends both on the material and the Vickers indentation fracture toughness expression used to calculate K_C. Rather, it was suggested[19] that a strong dependence of K_C on $a^{1/2}$ is indicative of a residual surface stress. However, the sign of the slope cannot be used to distinguish between a residual compressive and a residual tensile surface stress without K_C vs. $a^{1/2}$ data for both the definite stress-free condition and the residual compressive or tensile stress condition in a given material type.[19]

Krause *et al.*[8] have reported a fracture resistance value of 5·35 ± 0·17 MPa $m^{1/2}$, measured by the indentation–strength method, in an earlier investigation on the same composite. In the indentation–strength method, strength tests were conducted in four-point bend loading with the Vickers indentation at the centre of the prospective tensile surface. The size of the radial cracks emanating from the Vickers indentation was controlled by varying the indentation load. For the same composite, these authors[8] used a parametric representation of the fracture resistance as a fractional power function in crack extension of the form:

$$K_R = K_O (\Delta C / C_O)^m \tag{3}$$

where K_R is a parameter describing the fracture resistance for an R-curve type material, m measures the relative steepness of the R-curve, K_O is the fracture resistance that corresponds to the smallest indentation crack radius, C_O is the smallest indentation crack that causes failure in flexural testing, ΔC is the crack extension (= $C - C_P$). The total crack length is C and C_P is the traction-free portion, such as exists in a pre-notched specimen. K_O and m are defined by:[8]

$$K_O = \beta^{-\beta}(1 + \beta)^{(1+\beta)} Y S_O C_O^{1/2} \tag{4}$$

$$m = (1 - 3\beta)(2 + 2\beta) \tag{5}$$

where the constant $\beta = 0{\cdot}266$, Y is the configuration coefficient and is equal to 1·174. S_O is the natural strength of the composite corresponding to the minimum indentation load P_O and is equal to 559 MPa. This is the maximum strength that could be measured for specimens with indentation cracks before failures from natural flaws dominate the strength distribution.

For their analysis,[8] indentation flaws were assumed to have traction from the outset, so $C_P = 0$. When $m = 0$, K_R is invariant with ΔC and $K_R = K_O = K_C$. The values of m, C_O and K_O for the same composite[8] were 0·08, 18·1 μm and 5·35 MPa $m^{1/2}$, respectively. Using the above expression, Fuller *et al.*[8] observed that the fracture resistance of the material K_R increases with crack extension, the so called rising R-curve phenomenon. This behaviour was explained in terms of the whiskers acting as elastic restraints to the point of rupture at small crack wall separations.

In the present study, the average value of indentation fracture toughness (Table 1) was reasonably in agreement with the fracture resistance value obtained by NIST.[8] Probably due to the non-uniform distribution of the SiC whiskers in the matrix of alumina [Fig. 1(b)], the value of K_C at a load of 1·2 kN was slightly high (Table 1 and Fig. 3). The average fracture toughness K_{IC} evaluated by using the precracked specimen was 5·96 ± 0·15 MPa $m^{1/2}$. The large difference in toughness obtained by the two methods could primarily be accounted for the difference in crack tip loading rates.

For many brittle materials, the indentation fracture toughness values were reported to be similar

to those obtained by large crack methods such as using a double cantilever beam[28] or compact tension[20,22] specimen. On the other hand, it was often contended that indentation toughness is a close approximation of the fracture from small, naturally occurring flaws.[8,28–32] However, one should make sure that the residual stress field, induced by the plastic zone[28] produced by the indentation, is small enough compared with the crack length that the indentation plastic zone has a minimum effect on the extension of cracks.

Previous investigators[8,30,33] have also reported that the considerable local branching at the corners of the indentation and small amount of deflection give rise to the appearance of local curvature in the crack path. The branching of cracks produced at the corners of the indentation was also observed in a previous study[34] and could partly account for the rising trend in the K_R (fracture resistance) values. This branching behaviour and the crack deflection observed (Figs 9 and 10) can also be explained in terms of a grain-bridging phenomenon associated with microstructural toughening. Possibly, on the scale of grain sizes, the grains of alumina were entangled with the silicon carbide whiskers in such a way that, because of the presence of a complex residual stress field, high resistance to crack propagation was created and hence the crack tended to find a new starting point at the weakest area away from this region.[29]

5.2 Fracture toughness of precracked specimens

The K_{IC} values determined using precracked four-point bend specimens could not readily be compared with those reported on this material by NIST,[8] due to the difference in the techniques used for determination of toughness. The scatter in the K_{IC} values obtained from the precracked specimens, shown in Table 1, could be due to the non-uniform distribution of the silicon carbide whiskers, apart from the system error inherent in the K_{IC} determination.

The plane of crack propagation in specimens tested was parallel to the LT plane. Since most of the whiskers were perpendicular to the crack plane, they would tend to bridge the crack plane more effectively and enhance the toughness. Therefore, the fracture toughness for the crack planes parallel to the hot-pressing direction (the L and ST planes) should be substantially higher than that for crack planes which are perpendicular to the hot-pressing direction. Hansson *et al.*[35] clearly showed that for 33 vol% SiC whisker reinforced alumina composite, the fracture toughness for crack planes parallel to the hot-pressing direction is substantially higher than that for perpendicular crack planes.

A Vickers hardness indentation introduced at a load of 0·8 kN was used as a crack starter. As a result, significant residual stresses could be induced in the specimen. If these residual stresses just ahead of the advancing crack front (i.e. within the plastic zone) were compressive in nature, they could decrease the observed fatigue crack growth rate and increase the observed K_{IC} of the material. However, if they were tensile in nature, the effect would be opposite. Some more fracture toughness tests, including those where a slot or notch is used as a crack starter, should be carried out to confirm and check the K_{IC} data reported in Table 1.

In a recent paper,[22] the K_{IC} value of 15 vol% (or 12·64% by weight) silicon carbide reinforced alumina ceramic composite using compact tension specimens was reported to be 4·5 MPa $m^{1/2}$. This toughness value is somewhat lower than the K_{IC} value determined by us. This difference could be attributed to a difference in the porosity of the materials, or in the amount or size of the silicon carbide whiskers used, or in the orientation of the crack plane or the specimen geometry. Also, as the whisker volume contents are different, the strength of the whiskers and the matrix–whisker interfacial bonding would obviously vary between the two test cases.

5.3 Fatigue crack growth rates

The results of the present study (Fig. 4) showed that 25 wt% silicon carbide whisker reinforced alumina ceramic composites were susceptible to the fatigue crack growth phenomenon, in a manner similar to metallic materials. FCGR data on 25 wt% silicon carbide reinforced alumina composite have not been reported earlier. However, recently, FCGR data of 15 vol% (which is equivalent to 12·64 wt%) silicon carbide alumina ceramic composite were given.[22] The crack growth rate in the material studied by us was about 100 times faster, at a given ΔK, than that in the other material, mainly due to larger porosity content in the former compared with the latter which is almost devoid of obvious processing flaws like porosity.[36] The difference could also be attributable to other factors, such as the strength of the whiskers and the matrix–whisker interfacial bonding.

Our material was observed to have much less resistance to fatigue than Ce-TZP–alumina composite[21] and MgO–PSZ composite.[20] As explained earlier,[20,21] the presence of the transformation zone ahead of the crack tip in these materials could result in the absorption of significant energy, and this could retard the observed fatigue crack growth rate.

Plots of da/dN vs. ΔK for the 12·64 wt% silicon carbide alumina composite and for the MgO–PSZ

composite exhibited a single linear stage with the exponent values of 15 and 28, respectively. Our material also exhibited a single linear stage (Fig. 4) without the presence of a detectable threshold. The value of the exponent was 15·5 in our material.

As already discussed, the Vickers hardness indentation when used as a crack starter could generate residual stresses which in turn could influence the FCGR. The FCGR test data on specimens where the crack starter is a slotted notch instead of an indentation, if generated, would confirm if the use of indentation as a crack starter indeed influences the FCGR or not. Such studies have been reported elsewhere.[15]

5.4 Mechanism of fracture

Since the mechanism of fracture of the whiskers and the α-alumina grains are entirely different in the low ΔK fatigue and the fast fracture regions, the scheme of crack growth in each region is discussed separately below to highlight these differences.[34]

During fatigue loading at low ΔK values, that is when $K_{max} < 2$ MPa $m^{1/2}$, the α-alumina grains of the matrix failed mainly by transgranular cleavage with frequent crack branching and crack deflection. Also, the cleavage facets revealed river patterns and steps. At the low values of ΔK, the K_{max} values are low. Consequently, the traction force ahead of the crack tip is not large enough to promote intergranular fracture.

At the same time, the whiskers could fail by three different modes: (i) pull out, (ii) tensile fracture and (iii) fatigue. Since only a few of the whiskers failed due to pull-out at low ΔK (see Fig. 5), this naturally indicates that the maximum traction forces generated ahead of the crack tip during the low ΔK fatigue was not adequate to produce pull-out. Thus it is likely that the whiskers continue to bridge the crack even after some of the surrounding alumina grains have failed by transgranular cleavage. Therefore, under these circumstances, the whiskers could fail due to tensile fracture or fatigue. Now, since the strength of the β-SiC whisker is about 6·5 to 7 times higher than that of α-alumina,[37,38] the tensile fracture of the whisker is unlikely if the traction forces ahead of the crack tip were to be distributed in proportion to the relative cross-sections of the β-SiC whiskers and α-alumina in the plane of the crack. Even if the whiskers were to carry the major part of the traction forces ahead of the crack tip, the high traction forces would produce failure by pull-out rather than by tensile fracture, as was observed in the fast fracture region (see Fig. 6) where K_{IC} values and consequently the traction forces were high. Since the possibility of large-scale pull-out or tensile fracture is thus discounted, whiskers are most likely to fail by fatigue. At low ΔK, the whiskers which had bridged the crack after the surrounding alumina grains had failed by cleavage, would continue to experience fatigue loading, then fail with a square fracture which is typical of fatigue.

During fast fracture under monotonic loading such as during the fracture toughness testing, 55% of the α-Al_2O_3 grains of the matrix failed by intergranular fracture. The value of K_I during such monotonic loading is 5·9 MPa $m^{1/2}$. At such values of K_I, the traction force ahead of the crack tip is adequate to produce intergranular failure of those grains which are favourably oriented with respect to it. The matrix failure was predominantly intergranular. Nevertheless, the whiskers were located mainly at the grain boundaries. Therefore the probability of the advancing crack front interacting with the whiskers is extremely high. The whiskers tending to bridge the advancing crack quite frequently would therefore become debonded and pull out. This hypothesis is confirmed by the fact that, during monotonic fracture, failure of the whiskers by the pull-out mechanism was frequently observed in the fractographs.

After some of the grains have failed by the intergranular mode, the other neighbouring grains—which are less favourably oriented or are bridged by the whiskers across the grain boundaries—fail by cleavage. The schematic of crack propagation during monotonic and cyclic loading is given elsewhere.[34]

To prevent fracture of this ceramic composite under monotonic loading, its microstructural features would have to be strengthened to avoid intergranular fracture of α-alumina and the pull-out of whiskers. This requires that the grain boundary strength of α-alumina and the whisker–matrix interfacial strength should be increased. Similarly, to retard crack extension during low ΔK fatigue, intergranular cleavage fracture of α-alumina grains and fatigue failure resistance of the silicon carbide whiskers should be improved, possibly by using finer α-alumina powder[13,14] and by improving the uniformity of distribution of the whiskers in the matrix during hot-pressing.[13,14]

6 Conclusions

The results of the foregoing study lead to the following conclusions.

(1) Indentation fracture toughness increased with increase in the square root of crack length. However, the K_{IC} values obtained

from the precracked four-point bend specimens were higher and had a value given by $K_{IC} = 5{\cdot}96 \pm 0{\cdot}15$ MPa $m^{1/2}$.

(2) The 25 wt% silicon carbide whisker reinforced alumina ceramic composite is susceptible to a fatigue crack growth phenomenon which is similar to that observed in the case of metallic materials. But the crack growth exponent is higher ($n = 15{\cdot}5$).

(3) At low ΔK fatigue (0·8 to 1·8 MPa $m^{1/2}$), the whiskers failed by fatigue, whereas during monotonic fracture, they failed by pull-out.

(4) The matrix at low ΔK fatigue was predominantly transgranular with frequent crack branching and deflection, in contrast to a mixed mode type (45% transgranular and 55% intergranular) failure during the monotonic fracture.

References

1. Becher, P. F., Hsueh, C. H., Angelini, P. & Tiegs, T. N., Toughening behaviour in whisker-reinforced ceramic matrix composites. *J. Am. Ceram. Soc.*, **71**(12) (1988) 1050–61.
2. Becher, P. F., Microstructural design of toughened ceramics. *J. Am. Ceram. Soc.*, **72**(2) (1991) 255–69.
3. Becher, P. F. & Tiegs, T. N., Toughening behaviour involving multiple mechanisms: whisker reinforcement and zirconia toughening. *J. Am. Ceram. Soc.*, **70**(9) (1987) 651–4.
4. Angelini, P., Mader, W. & Becher, P. F., Strain and fracture in whisker reinforced ceramics. In *MRS Proceedings Vol. 78, Advanced Structural Ceramics*, ed. P. F. Becher, M. V. Swain and S. Somuja. Materials Research Society, Pittsburgh, PA, 1987, pp. 241–57.
5. Ruhle, M., Dalgeish, B. J. & Evans, A. G., On the toughening of ceramics by whiskers. *Scr. Metall.*, **21** (1987) 681–6.
6. Warren, R. & Sarin, V. K., Fracture of whisker reinforced ceramics. In *Application of Fracture Mechanics to Composite Materials*, ed. K. Friedrich. Elsevier, Amsterdam, in press.
7. Krause Jr, R. F. & Fuller Jr, E. R., Fracture toughness behaviour of a silicon carbide whisker reinforced alumina with selected properties. In *Proc. the Fossil Energy Materials Conference, Report No. ORNL/FMP/87/G*, Martin Marietta Energy Systems, Inc., Oak Ridge National Laboratory, TN, USA, August 1987, pp. 38–55.
8. Krause Jr, R. F., Fuller Jr, E. R. & Rhodes, J. F., Fracture resistance behaviour of silicon carbide whisker-reinforced alumina composites with different porosities. *J. Am. Ceram. Soc.*, **73**(3) (1990) 559–66.
9. Campbell, G. H., Ruhle, M., Dalgleish B. J. & Evans, A. G., Whisker toughening: a comparision between Al_2O_3 and Si_3N_4 toughened with silicon carbide. *J. Am. Ceram. Soc.*, **73**(3) (1990) 521–30.
10. Solomah, A. C. & Reichert, W., Mechanical properties, thermal shock resistance and thermal stability of zirconia-toughened alumina–10 vol% silicon carbide whisker ceramic matrix composite. *J. Am. Ceram. Soc.*, **73**(3) (1990) 740–3.
11. Porter J. R. & Chokshi, A. H., Creep performance of SiC-whisker reinforced alumina. In *Ceramic Microstructure '86*, ed. J. A. Pask and A. G. Evans. Plenum Press, New York, 1986, pp. 919–28.
12. Tiegs, T. N. & Becher, P. T., Thermal shock behaviour of an alumina SiC whisker composite. *J. Am. Ceram. Soc.*, **70**(5) (1987) C-109–11.
13. Becher, P. F. & Wei, G. C., Toughening behaviour in SiC-whisker-reinforced alumina. *J. Am. Ceram. Soc.*, **67**(12) (1984) 267–9.
14. Wei, G. C. & Becher, P. F., Development of SiC whisker-reinforced ceramics. *J. Am. Ceram. Soc. Bull.*, **64**(2) (1985) 298–304.
15. Ray, A. K. & Banerjee, S., An articulated bridge fixture for precracking ceramic specimens in fatigue crack growth rate studies of 25 wt% SiC reinforced Al_2O_3 composite. *J. Am. Ceram. Soc.*, accepted.
16. Brown Jr, W. F. & Srawley, J. E., in *ASTM STP 410*. American Society for Testing and Materials, Philadelphia, PA, 1966.
17. Yamade, Y. & Kishi, T., Acoustic emission study for fracture origin of sintered mullite in 4-point bending test. *The Sumitomo Search*, **45**(3) (1991) 17–24.
18. Anstis, G. R., Chantikul, P., Lawn, B. R. & Marshall, D. B., A critical evaluation of indentation techniques for measuring fracture toughness: I, direct crack measurement. *J. Am. Ceram. Soc.*, **64** (1981) 533–8.
19. Ponton, C. B. & Rawlings, R. D., Dependence of the Vickers indentation, fracture toughness on the surface crack length. *Br. Ceram. Trans. J.*, **88** (1989) 83–90.
20. Dauskardt, R. H., Marshall, D. B. & Ritchie, R. O., Cyclic fatigue-crack propagation in magnesia–partially stabilized zirconia ceramics. *J. Am. Ceram. Soc.*, **73**(4) (1990) 893–903.
21. Tsai, J. F., Yu, C. S. & Shetty, D. K., Fatigue crack propagation in ceria-partially stabilized zirconia (Ce-TZP)–alumina composites. *J. Am. Ceram. Soc.*, **73**(10) (1990) 2992–3001.
22. Dauskardt, R. H., James, M. R., Porter, J. R. & Ritchie, R. O., Cyclic fatigue crack growth in a SiC whisker-reinforced alumina ceramic composite: long and small crack behaviour. *J. Am. Ceram. Soc.*, **75**(4) (1992) 759–71.
23. Lange, F. F., James, M. R. & Green, D. J., Determination of residual stresses caused by grinding in polycrystalline Al_2O_3. *J. Am. Ceram. Soc.*, **66** (1983) C-16–7.
24. Cook, R. F., Lawn, B. R., Dabbs, T. P. & Chantikul, P., Effect of machining damage on the strength of a glass ceramic. *J. Am. Ceram. Soc.*, **64** (1981) C-121–2.
25. Green, D. J., Lange, F. F. & James, M. R., Factors influencing residual surface stresses due to a stress-induced phase transformation. *J. Am. Ceram. Soc.*, **66** (1983) 623–9.
26. Marshall, D. B. & Lawn, B. R., An indentation technique for measuring stresses in tempered glass – surfaces. *J. Am. Ceram. Soc.*, **60** (1977) 86–7.
27. Ikuma, Y. & Virkar, A. V., Crack-size dependence of fracture toughness in transformation – toughened ceramics. *J. Mater. Sci.*, **19** (1984) 2223–8.
28. Bhattacharya, A. K. & Petrovic, J. J., Hardness and fracture toughness of SiC-particle-reinforced $MoSi_2$ composite. *J. Am. Ceram. Soc.*, **74**(10) (1991)) 2700–3.
29. Swanson, P. L., Fairbanks, C. J., Lawn, B. R. Mai, Y. W. & Hockey, B. J., Crack-interface grain bridging as a fracture resistance mechanism in ceramics: I, experimental study in alumina. *J. Am. Ceram. Soc.*, **70**(4) (1987) 279.
30. Ramchandran, N. & Shetty, D. K., Rising crack growth resistance (*R*-curve) behaviour of toughened alumina and silicon nitride. *J. Am. Ceram. Soc.*, **74**(10) (1991) 2634–41.
31. Anderson, R. M. & Braun, L. M., Technique for the *R*-curve determination of Y-TZP using indentation–produced flaws. *J. Am. Ceram. Soc.*, **73**(10) (1990) 3059–62.
32. Swain, M. V., *R*-curve behaviour and thermal shock resistance of ceramics. *J. Am. Ceram. Soc.*, **73**(3) (1990) 621–8.
33. Pezzotti, G., Tanaka, I. & Okamoto, T., Si_3N_4/SiC-whisker composites without sintering aids: 11, fracture behaviour. *J. Am. Ceram. Soc.*, **73**(10) (1990) 3039–45.
34. Ray, A. K., Das, S. K. & Banerjee, S., Fractography of the fatigued and fractured regions in a silicon carbide whisker reinforced alumina composite. *J. Eur. Ceram. Soc.*, **15** (1995) 191–9.
35. Hansson, T., Warren, R. & Wasen, J., Fracture tough-

ness mechanisms of a hot-pressed alumina reinforced with silicon carbide whiskers. *J. Am Ceram. Soc.*, **76**(4) (1993) 841–8.
36. Porter, J. R., Lange, F. F. & Chokshi, A. H., Processing and creep performance of SiC-whisker-reinforced Al_2O_3. *J. Am. Ceram. Soc. Bull.*, **66**(2) (1987) 343–7.
37. Fisher, E. S., Manghanani, M. H. & Routbort, J. L., Study of the elastic properties of Al_2O_3 and Si_3N_4 material composites with SiC whisker reinforcement. In *High Performance Composites for the 1990's*, ed. S. K. Das, C. P. Ballard and F. Marikar. The Minerals, Metals and Materials Society, 1991, p. 365.
38. Anon., Reinforcing tomorrows technology. *Ceram. Indust.*, April 1992.